Electrochemical Reaction Engineering of Polymer Electrolyte Fuel Cell

M. Kawase, K. Sato, R. Mitsui, H. Asonuma, M. Kageyama, K. Yamaguchi, and G. Inoue
Kyoto University, Kyotodaigaku-Katsura, Nishikyo-Ku, Kyoto 6158510, Japan

DOI 10.1002/aic.15545
Published online November 1, 2016 in Wiley Online Library (wileyonlinelibrary.com)

Although fuel cells can be considered as a type of reactor, methods of kinetic analysis and reactor modeling from the viewpoint of chemical reaction engineering have not yet been established. The rate of an electrochemical reaction is a function of concentration, temperature, and interfacial potential difference (or electromotive force). This study examined the cathode reaction in a polymer electrolyte fuel cell, in which oxygen and protons react over platinum in the catalyst layer (CL). The effects of the oxygen partial pressure and the cathode electromotive force on the reaction rate were assessed. Resistance to proton transport increases the electromotive force and reducing the reaction rate. It was established that the effectiveness factor of the cathode CL is determined by competition between the reaction and mass transport of oxygen and protons. Two dimensionless moduli that govern the cathode behavior are proposed as a means of depicting the processes in the cell. © 2016 American Institute of Chemical Engineers *AIChE J*, 63: 249–256, 2017
Keywords: polymer electrolyte fuel cell, modeling, oxygen reduction reaction rate, cathode electromotive force

Introduction

Polymer electrolyte fuel cells (PEFCs) have been developed to the point where they allow low-temperature operation and daily starting and stopping, and thus have been commercialized in practical applications. However, further improvements in the efficiency of these devices are required for cost reduction purposes. The greatest single contribution to the cost of a PEFC is the platinum catalyst, and so optimization of the cathode design and hence modeling of the cathode are required.

The rate of a chemical reaction is a function solely of the reactant concentrations and the temperature, while the rate of an electrochemical reaction is affected by the same factors but also the interfacial potential difference (that is, the electromotive force or emf). Although incorporating emf into the modeling of such reactions is complicated, the emf is considered a vital intrinsic parameter capable of controlling the reaction rate but yet unexplored from the viewpoint of chemical reaction engineering.

A design-for-purpose PEFC model is required to optimize the catalyst layer (CL) design.[1] As shown in Figure 1, a PEFC employs a gas-diffusion electrode and the cathode CL is composed of carbon black particles that support platinum nanoparticles, an ionomer (an ion-conductive polymer) that binds the Pt/carbon black particles, and pores. The O_2 pressure and the H^+ potential profiles are determined by the resistance of the pores to O_2 transport and by the resistance of the ionomer to H^+ transport, respectively, if no water is condensed.

Although many studies concerning PEFC modeling have been published,[2] most have involved direct numerical simulations of the device. The functioning of a PEFC, especially that of the cathode, remains complicated. The objective of this study was to develop two dimensionless moduli that explain the cathode behavior based on theoretical considerations on the O_2 partial pressure reduced by the O_2 transport resistance and the H^+ potential lowered by the H^+ transport resistance, as well as to demonstrate the manner in which these dimensionless moduli affect the reaction rate profile in the PEFC cathode layer and the catalyst effectiveness factor. These moduli can be used to characterize a variety of CL structures and to quantitatively determine differences in operating conditions. Although an isothermal cathode model is described in this study, the effects of energy transport and temperature profile are also important.[1]

Experimental

In this work, kinetic data were acquired using a single symmetric fuel cell. A Nafion® NRE-211 membrane (25.4 μm thick) and CLs made of Pt/graphitized Ketjenblack® catalyst (Pt/C weight ratio = 0.5) with a Nafion ionomer (ionomer/carbon weight ratio = 0.9) were installed. Platinum loadings of 0.13, 0.22, 0.31, 0.36, and 0.72 mg/cm^2 were employed in the thickness dependency measurements, in conjunction with respective thicknesses of 3.3, 5.6, 8.7, 10.1, and 18.6 μm. The active area was 2.0 cm $\times$ 2.0 cm. Carbon paper (Toray TGP-H-060) was used as the gas diffusion layer (GDL) which was 9.8–13% compressed in the cell. A 251 mm long, 1 mm wide, and 1 mm deep single serpentine gas flow channel was grooved in a carbon current collector. The width of ribs between legs of the gas channel was 1 mm. The cell was operated under atmospheric pressure at 80°C in a constant temperature and constant humidity oven. Undiluted H_2 and undiluted O_2 or O_2 diluted in nitrogen were humidified and supplied to

Correspondence concerning this article should be addressed to M. Kawase at kawase@cheme.kyoto-u.ac.jp.

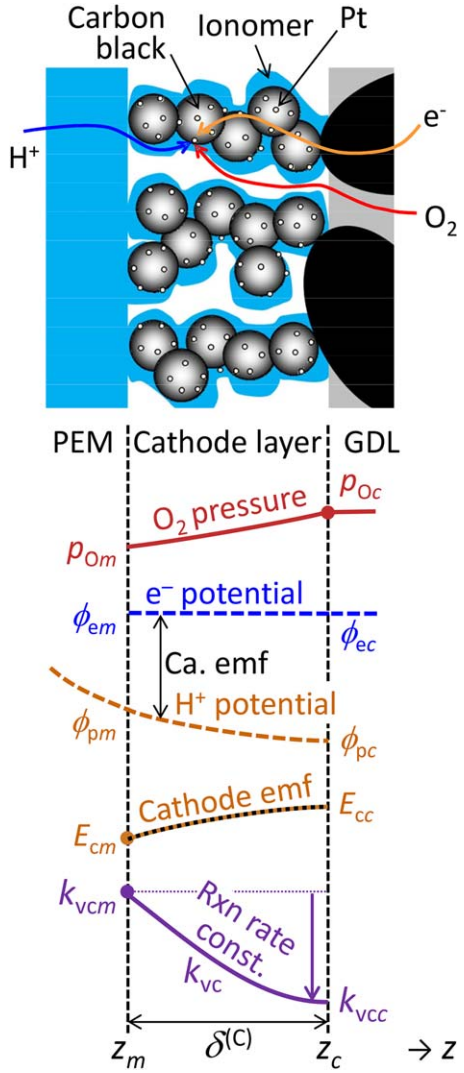

Figure 1. Structure of the PEFC cathode and reaction rate profile.

[Color figure can be viewed at wileyonlinelibrary.com]

the cell at flow rates high enough to ensure a low O_2 consumption of 10% at a current density of 2 A/cm^2. The H_2 and O_2 flow rates were, respectively, 600 and 300 cm^3/min (20°C, 1 atm) on dry basis. Data for use in kinetic analysis were acquired at current densities below 0.6 A/cm^2 at fractional O_2 consumptions less than 3%. Due to the water formation associated with the fuel cell reaction, the relative humidity (RH) at the outlet of the cell increased to just below 80% when the RH at the inlet was 75%. Based on estimations of water vapor saturation, no water condensation was expected at current densities below 2.57 A/cm^2 under the experimental conditions employed in these trials.

Polarization curves were obtained and electrochemical impedance spectroscopy was carried out using an electrochemical measurement system (Hokuto Denko Corp., HZ-5000). A standard equivalent circuit model was employed to determine the membrane resistance[3] and the measured membrane resistivity values were 0.23, 0.29, 0.34, and 0.37 Ω m at RH values of 81.4, 65.8, 52.8, and 33.2%. The measured cell voltage combined with the membrane resistance overpotential (the IR-corrected cell voltage) was regarded as the cathode emf, E_{cm}, at the membrane–CL boundary.

Experimental Results

Polarization curves were used to determine the rate of the oxygen reduction reaction (ORR):

$$O_2 + 4H^+ + 4e^- \rightarrow 2H_2O. \quad (1)$$

It has been shown that the mass transport resistance can be eliminated if the CL is thinner than 6 μm when operating under highly humid conditions.[4] Thus, to lower the mass transport resistance, the thickness of the cathode CL was reduced. As the thickness was reduced, the rate per unit amount of platinum increased and eventually plateaued, and this value was taken as equal to the intrinsic reaction rate that is defined as the reaction rate expected assuming no resistances to transports in the through-plane direction of the CL.

The ORR rates obtained with a 3.3 μm-thick CL are plotted in Figure 2, from which it is evident that the ORR rate was proportional to the oxygen partial pressure. The linearity of this relationship at a constant cathode emf was verified up to 220 kPa in experiments under elevated pressure.[5] A first-order reaction rate expression was employed to represent the dependency of the ORR rate on the O_2 partial pressure in this study. It should be noted that the overpotential will vary with the oxygen partial pressure, thus any measurements at a fixed voltage or a fixed current do not give rate data at an identical cathode emf. The data must be acquired at the same emf from a series of polarization curve measurements to establish the reaction order.

Figure 3 summarizes the first-order ORR rate constants,[6] from which it can be seen that the constants can be plotted as exponential functions of the cathode emf. This result establishes that the Tafel equation can be applied to these data. Depending on the potential region, two trend lines are evident, as the result of oxidation of the platinum surfaces at high potentials.[7,8] The relationship between the ORR rate constant

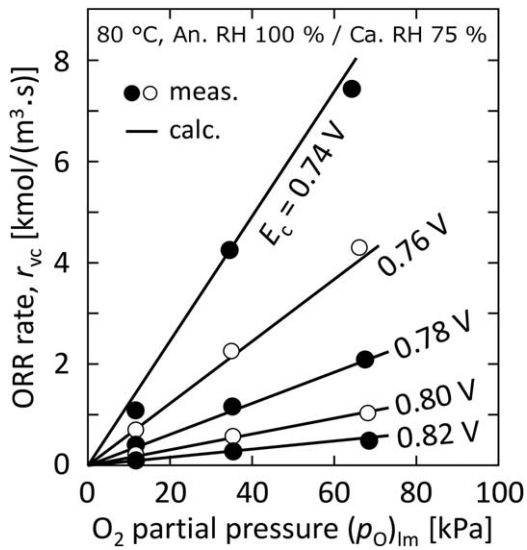

Figure 2. Dependency of the ORR rate on oxygen partial pressure (Pt 388 kg/m^3, $(p_O)_{lm}$ is the logarithmic mean of inlet and outlet oxygen partial pressures).

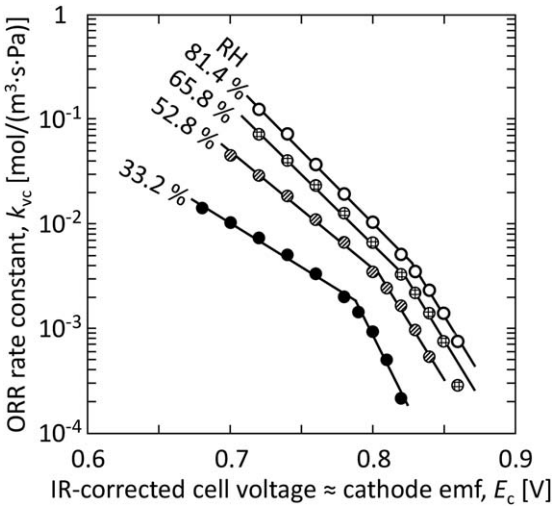

Figure 3. Dependency of the ORR rate on cathode emf (Pt 359 kg/m^3, 80°C, An. RH = Ca. RH).

and the cathode emf (in this case, at an RH of 81.4%) can be expressed as:

$$k_{vc} = 1.39 \times 10^9 \,\mathrm{mol \cdot m^{-3} \cdot s^{-1} \cdot Pa^{-1}} \exp\left(-\frac{E_c}{0.0313\ \mathrm{V}}\right). \tag{2}$$

Although the slope and intercept will vary with the specific RH, the Tafel equation is valid for reduced platinum under all conditions. In the theoretical model in this work, a single Tafel equation was employed to represent the dependency of the ORR rate on the cathode emf. The first-order rate constant determined above may include the effect of the resistance of the ionomer to O_2 transport from the gas phase in the pores to platinum, which cannot be separated at the moment.

Theoretical Model

The ORR rate per unit volume of cathode CL, r_{vc}, in Eq. 1 is generally expressed as follows:

$$r_{vc} = k_{vc}^{\oplus} \exp\left(-E_c/b_c\right) p_O \,[\mathrm{mol/(m^3 \cdot s)}], \tag{3}$$

where E_c is the cathode emf, b_c is the Tafel slope, $k_{vc}^{\oplus}$ is the reaction rate constant at $E_c = 0$, and p_O is the partial pressure of oxygen. Since the proton concentration in the ionomer is much higher than the oxygen concentration, it can be regarded as a constant and is therefore included in the reaction rate constant. The proton transport resistance affects the reaction rate not by reducing the proton concentration but by reducing the proton potential and increasing the cathode emf.

To predict the profile of the ORR rate in the CL, both the distribution of O_2 and the cathode emf are required and this study employs an isothermal one-dimensional model for this purpose. No crossover of gas through the proton exchange membrane (PEM) and no condensation of water vapor in the CL are assumed.

The material balance of oxygen leads to the following fundamental equation:

$$dN_O/dz = -r_{vc}, \tag{4}$$

where z is the location in the through-plane direction defined in Figure 1, and N_O is the absolute oxygen flux. This latter term is the sum of the convection term and the diffusion term, as follows:

$$N_O = N_g y_O - C_g D_{eO}\, dy_O/dz, \tag{5}$$

where y_O is the mole fraction of oxygen, D_{eO} is the effective oxygen diffusivity, C_g is the total gas molar concentration, and N_g is the total gas flux. N_g is the sum of the fluxes of oxygen and water vapor, since the nitrogen flux is zero even when air is supplied to a cell. Although Eq. 5 is a diffusion rate equation for the binary component system rather than the Maxwell–Stefan equation, binary diffusivity in a multicomponent system can be employed in the case that the gas being supplied is air.[9]

Considering the reaction stoichiometry between N_O and the water vapor flux, N_S, in the region from z_m to z, we can write:

$$(N_O - 0)/(-1) = \left(N_S - N_A^{(M)}\right)\Big/2, \tag{6}$$

where $N_A^{(M)}$ is the water flux through the PEM, equal to the water vapor flux at the PEM–CL boundary. Therefore, the total gas flux can be expressed as follows:

$$N_g = N_A{}^{(M)} - N_O. \tag{7}$$

The water flux through the membrane is determined by the drag and diffusion through the PEM. In this study, $N_A^{(M)}$ is regarded as an operating condition since, in addition to the membrane properties, its value depends on the humidity supplied to both the anode and cathode, as well as the current density.

The boundary conditions are zero flux at the PEM–CL boundary and a given mole fraction at the CL–GDL boundary, as follows:

$$N_O = 0 \text{ at } z = z_m \text{ and } y_O = y_{Oc} \text{ at } z = z_c. \tag{8}$$

The proton flux, N_p, varies according to the ORR as in the equation:

$$dN_p/dz = -4r_{vc}. \tag{9}$$

Protons are primarily transported as the result of electrostatic drag, and so the proton flux can be expressed as:

$$FN_p = -\sigma_{ep} d\phi_p/dz, \tag{10}$$

where F is the Faraday constant, σ_{ep} is the effective proton conductivity [S/m], and ϕ_p is the proton potential. The cathode emf, E_c, is the difference between the electron potential and the proton potential ($\phi_e - \phi_p$). The electron potential can be assumed constant through the cathode CL, and therefore the relationship between the differential of ϕ_p and the differential of E_c is $d\phi_p = -dE_c$. Since only a single reaction is considered, the proton flux can be calculated from the reaction stoichiometry. Eliminating r_{vc} by coupling Eqs. 4 and 9, the following equation is derived:

$$4F(N_O - N_{Oc}) = \sigma_{ep} dE_c/dz, \tag{11}$$

where N_{Oc} is the oxygen flux at the CL–GDL boundary. The boundary condition consists of a given cathode emf at the PEM–CL boundary, as follows:

$$E_c = E_{cm} \text{ at } z = z_m. \tag{12}$$

This system of fundamental equations has 22 terms and 12 degrees of freedom. Out of these terms, 11 values need to be specified to determine the oxygen partial pressure and cathode

emf profiles. This large number of variables obviously makes it difficult to understand the behavior of the PEFC cathode. However, if these fundamental equations are converted to dimensionless equations, dimensionless solutions can be determined based on dimensionless moduli defined as ratios of kinetic parameters, rather than using the values of the kinetic parameters themselves.

Dimensionless Model Description

In this work, distance, partial pressure, molar flux, and cathode emf were, respectively, normalized by the cathode CL thickness, $\delta^{(C)}$, the O_2 partial pressure at the CL–GDL boundary, p_{Oc}, the typical diffusive flux, $C_g D_{eO} y_{Oc}/\delta^{(C)}$, and the Tafel slope, b_c. Hence, the dimensionless location, ζ, the dimensionless oxygen partial pressure, π_O, the dimensionless oxygen flux, v_O, and the dimensionless cathode emf, ε_c, are defined as follows:

$$\zeta = (z - z_m)/(z_c - z_m) = (z - z_m)/\delta^{(C)}, \tag{13}$$

$$\pi_O = p_O/p_{Oc}, \tag{14}$$

$$v_O = N_O\,\delta^{(C)}/\left(C_g D_{eO} y_{Oc}\right) \text{ and} \tag{15}$$

$$\varepsilon_c = (E_c - E_{cm})/b_c. \tag{16}$$

The dimensionless cathode emf, ε_c, is equal to the dimensionless proton potential drop, $(\phi_{pm} - \phi_p)/b_c$, since $d\phi_p = -dE_c$.

The oxygen flux in Eq. 5 is converted to the following dimensionless form:

$$v_O = \frac{1}{1 + y_{Oc}\pi_O}\left(P^{(C)}_{O\,m}\pi_O - \frac{d\pi_O}{d\zeta}\right), \tag{17}$$

where $P^{(C)}_{O\,m}$ is the Peclet number, defined at the PEM–CL boundary as follows:

$$P^{(C)}_{O\,m} = \frac{\delta^{(C)} N^{(M)}_A}{C_g D_{eO}}. \tag{18}$$

The oxygen balance in Eq. 4 in conjunction with the rate in Eq. 3 is converted into the following dimensionless form:

$$\frac{dv_O}{d\zeta} = -M^{(C)^2}_{O\,m}\pi_O \exp(-\varepsilon_c), \tag{19}$$

$$\text{where } M^{(C)}_{O\,m} = \delta^{(C)}\sqrt{\frac{k^{\oplus}_{vc}\exp(-E_{cm}/b_c)p_{Oc}}{C_g D_{eO} y_{Oc}}}. \tag{20}$$

Here, a dimensionless modulus, a sort of Thiele modulus, appears. This modulus represents the ratio of typical reaction and oxygen diffusion rates, as described below:

$$M^{(C)\,2}_{O\,m} = \frac{\delta^{(C)} k^{\oplus}_{vc} p_{Oc}\exp(-E_{cm}/b_c)}{C_g D_{eO}(y_{Oc} - 0)/\delta^{(C)}} = \frac{\text{Reaction rate w/o } O_2 \text{ \& } H^+ \text{ transport resistance}}{\text{Typical } O_2 \text{ diffusion rate}}. \tag{21}$$

The boundary conditions in Eq. 8 are converted as follows:

$$v_O = 0 \text{ at } \zeta = 0 \text{ and } \pi_O = 1 \text{ at } \zeta = 1. \tag{22}$$

The symbols representing the boundaries disappear owing to the definition of the dimensionless variables ζ and π_O.

The reaction stoichiometry, combined with the proton transport rate equation, Eq. 11, is converted to the following dimensionless form:

$$v_O - v_{Oc} = \frac{M^{(C)^2}_{O\,m}}{M^{(C)\,2}_{p\,m}}\frac{d\varepsilon_c}{d\zeta}, \tag{23}$$

$$\text{where } M^{(C)}_{p\,m} = \delta^{(C)}\sqrt{\frac{4F k^{\oplus}_{vc} p_{Oc}\exp(-E_{cm}/b_c)}{\sigma_{ep} b_c}}. \tag{24}$$

Here v_{Oc} is the dimensionless oxygen flux at the CL–GDL boundary.

Another dimensionless modulus appears in Eq. 23. It is proposed to employ this modulus, $M^{(C)}_{p\,m}$, for representing the resistance to proton transport by the potential gradient. This modulus represents the ratio of reaction to proton transport as in the equation:

$$M^{(C)\,2}_{p\,m} = \frac{\delta^{(C)} k^{\oplus}_{vc} p_{Oc}\exp(-E_{cm}/b_c)[(E_{cc} - E_{cm})/b_c]}{\sigma_{ep}(\phi_{pm} - \phi_{pc})/(4F\delta^{(C)})}. \tag{25}$$

The denominator in this expression is the average proton transport rate whereas the numerator is the product of the differential coefficient of the intrinsic reaction rate with respect to the cathode emf and the difference between the cathode emf values at either end of the CL. This factor is required since the intrinsic reaction rate is not proportional to the cathode emf itself.

The boundary condition in Eq. 12 actually disappears owing to the definition of the dimensionless cathode emf, ε_c, as follows:

$$\varepsilon_c = 0 \text{ at } \zeta = 0. \tag{26}$$

This dimensionless system consists of nine terms and four equations (Eqs. 17, 19, 23, and Eq. 17) at $\zeta = 1$ (the CL–GDL boundary)), and has five degrees of freedom. The degrees of freedom are greatly reduced by employing the dimensionless forms of the model equations. Only four values ($M^{(C)}_{O\,m}$, $M^{(C)}_{p\,m}$, $P^{(C)}_{O\,m}$, and y_{Oc}) need to be specified to determine the dimensionless oxygen partial pressure profile and the dimensionless cathode emf profile, and the proposed dimensionless moduli have clear meanings, as described above.

The catalyst effectiveness factor is defined as the ratio of the actual reaction rate to the intrinsic reaction rate, assuming no transport resistance. The effectiveness factor, $F^{(C)}_e$, is then calculated by the following equation:

$$F^{(C)}_e = \int_0^1 \pi_O e^{-\varepsilon_c} d\zeta = \frac{-N_{Oc}}{\delta^{(C)} k_{vcm} p_{Oc}} = \frac{-v_{Oc}}{M^{(C)^2}_{O\,m}}. \tag{27}$$

The effects of the dimensionless moduli $M^{(C)}_{O\,m}$ and $M^{(C)}_{p\,m}$ on the reaction are illustrated in Figure 4. When the transport resistance is negligible, the reaction evidently proceeds with an effectiveness factor close to 1. As the oxygen transport resistance increases, oxygen is depleted in the region far from the oxygen inlet, the CL–GDL boundary, and consequently the effectiveness factor is reduced. In the case that the proton transport resistance is high, the proton potential is greatly lowered near the GDL, and hence the cathode emf is raised, reducing both the reaction rate and the effectiveness factor.

The dimensional current density is calculated as follows:

$$i = 4F\,\delta^{(C)} k_{vcm}\, p_{Oc}\, F_e{}^{(C)}, \tag{28}$$

where $k_{vcm}\, p_{Oc}$ is the intrinsic ORR rate. As far as values of the dimensionless moduli are known, $F^{(C)}_e$ is given and therefore the current density can be calculated without solving the differential equations. The proposed cathode model is valid as

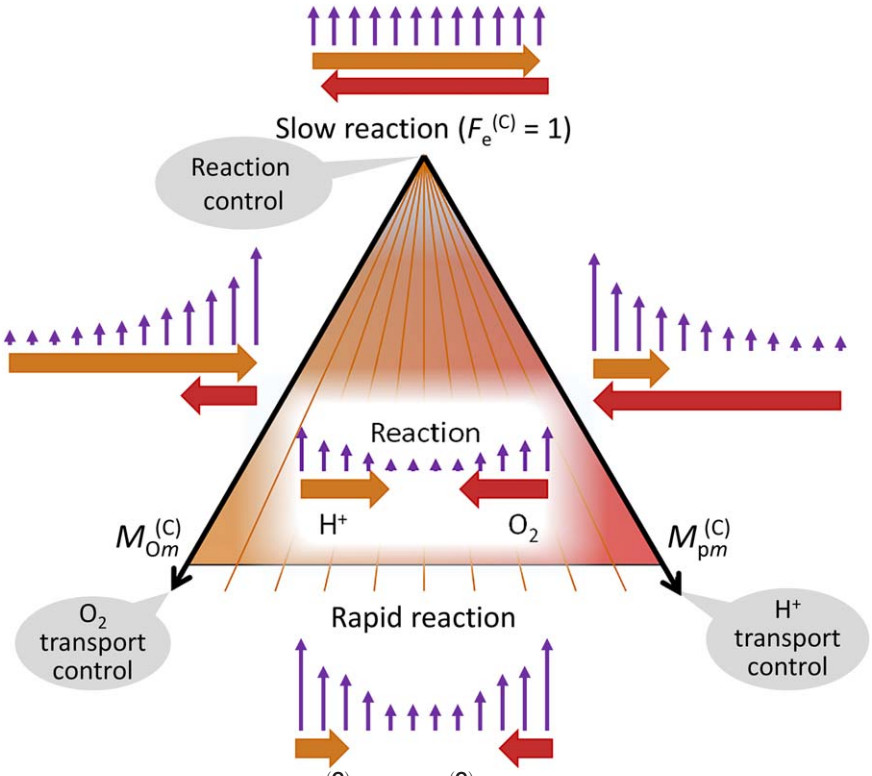

Figure 4. Effects of the dimensionless moduli $M_{O\,m}^{(C)}$ and $M_{p\,m}^{(C)}$ on reaction.

[Color figure can be viewed at wileyonlinelibrary.com]

far as the ORR rate is of the first order with respect to the O_2 partial pressure, the Tafel equation represents the ORR rate dependency on the cathode emf, and no water is condensed. Although the O_2 distribution and the H^+ potential drop in the CL are represented by the proposed cathode model, it has to be combined with the models of the other layers to assess the cell performance unless completely under the reaction control conditions. Conditions of the other layers affect the intrinsic ORR rate in Eq. 28 besides the values of the dimensionless moduli. For instance, the PEM conditions alter the cathode emf, E_{cm}, and the ORR rate constant, k_{vcm}, at the PEM–CL boundary. The GDL conditions affect the O_2 partial pressure, p_{Oc}, and the O_2 mole fraction, y_{Oc}, at the CL–GDL boundary.

Dimensionless Model Analysis

The dimensionless model equations were numerically solved according to the following algorithm: (1) assuming an initial profile for the dimensionless cathode emf (ε_c vs. ζ), (2) finding the dimensionless oxygen partial pressure profile (π_O vs. ζ) by solving Eq. 19 with Eq. 17, using a finite difference method, (3) determining ε_c vs. ζ through integrating Eq. 23, and (4) repeating steps (2) and (3) until the ε_c profile converges. Since Eq. 19 is nonlinear, iterative calculations are also required in step (2). This nonlinearity originates from the denominator $1 + y_{Oc}\pi_O$ in Eq. 17.

Figures 5a–c show the profiles of the dimensionless oxygen partial pressure, cathode emf and reaction rate at $M_{O\,m}^{(C)} = 1$ and $M_{p\,m}^{(C)} = 0.411$, 1, and 4.11, respectively, in the case that oxygen convection is negligible compared with the diffusion rate ($P_{O\,m}^{(C)} = 0.1$, $y_{Oc} = 0.62$). Since the oxygen transport resistance is not negligible at $M_{O\,m}^{(C)} = 1$, the oxygen partial pressure decreases toward the PEM–CL boundary moving away from the oxygen inlet (the CL–GDL boundary). The proton transport resistance raises the cathode emf near the CL–GDL boundary. As $M_{p\,m}^{(C)}$ increases, the proton transport resistance increases compared with the reaction resistance. In the case shown in Figure 5c, the dimensionless cathode emf increases to 1.72 at the CL–GDL boundary, that is the H^+ potential drop is 1.72 times as great as the Tafel slope. If the ORR rate is expressed by Eq. 2, the potential drop is estimated as 54 mV. The reaction rate constant at the CL–GDL boundary is 5.7 times lower than at the PEM–CL boundary due to the increased cathode emf. Although the oxygen partial pressure is higher near the GDL than near the PEM, the decrease in the reaction rate constant overtakes the increase in the oxygen partial pressure and the reaction rate becomes lower near the GDL. The dimensionless reaction rate is highest at the PEM–CL boundary ($\zeta = 0$) when $M_{p\,m}^{(C)}$ dominates, while the dimensionless reaction rate is highest at the CL–GDL boundary ($\zeta = 1$) when $M_{O\,m}^{(C)}$ dominates. When $M_{O\,m}^{(C)}$ and $M_{p\,m}^{(C)}$ are comparable, a minimum reaction rate is exhibited in the CL, as shown in Figure 5b.

The shaded areas in Figures 5a–c represent values of the effectiveness factor, $F_e^{(C)}$, and this term is plotted as a function of $M_{O\,m}^{(C)}$ and $M_{p\,m}^{(C)}$ ($P_{O\,m}^{(C)} = 0.1$, $y_{Oc} = 0.62$) in Figure 6. As expected, $F_e^{(C)}$ is reduced by increased transport resistance. Because $M_{O\,m}^{(C)}$ is relatively high in the low $M_{p\,m}^{(C)}$ region, $F_e^{(C)}$ exhibits a plateau of sorts, since the oxygen transport resistance is so high that most of the transport resistance can be ascribed to oxygen transport, and the proton transport resistance becomes negligible compared with the oxygen transport resistance. On the contrary, $F_e^{(C)}$ is affected more by $M_{p\,m}^{(C)}$ when $M_{O\,m}^{(C)}$ is low. The ratio of $F_e^{(C)}$ at $M_{p\,m}^{(C)} = 0.1$ to that at $M_{p\,m}^{(C)} = 10$ is 7.0 for $M_{O\,m}^{(C)} = 0.1$ and 3.2 for $M_{O\,m}^{(C)} = 5$. In any case, the effectiveness factor appears inversely proportional to $M_{p\,m}^{(C)}$ as $M_{p\,m}^{(C)}$ approaches infinity. As typically seen in the effectiveness factor–Thiele modulus relationship, the

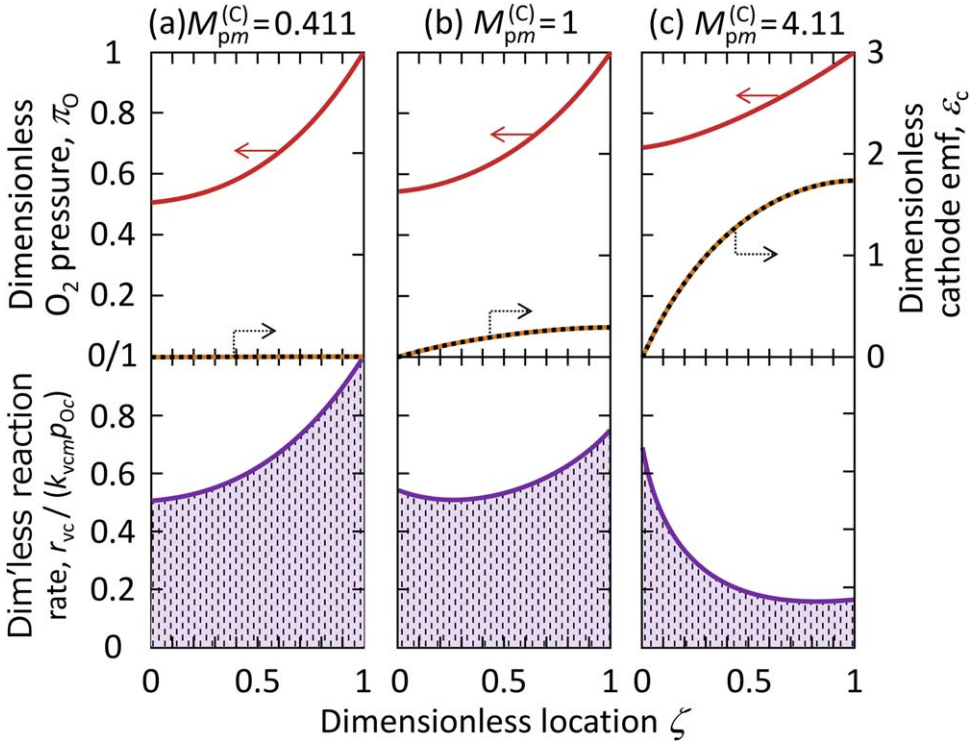

Figure 5. Profiles of dimensionless oxygen partial pressure, dimensionless cathode emf, and dimensionless reaction rate at $M_{O\,m}^{(C)} = 1$: (a) $M_{p\,m}^{(C)} = 0.411$, (b) $M_{p\,m}^{(C)} = 1$, (c) $M_{p\,m}^{(C)} = 4.11$ ($P_{O\,m}^{(C)} = 0.1$).

[Color figure can be viewed at wileyonlinelibrary.com]

asymptotes at both extremes, 0 and infinity, cross at approximately $M_{p\,m}^{(C)} = 1$.

Figure 7 shows the $F_e^{(C)}$ contours in an $M_{O\,m}^{(C)} - M_{p\,m}^{(C)}$ plot calculated with no convection effects ($P_{O\,m}^{(C)} = 0$, $y_{Oc} = 0.62$). This is a quantitative representation of the relationship between $F_e^{(C)}$ and the dimensionless moduli previously presented in Figure 4. The left lower region of the graph in Figure 7 corresponds to the upper part of Figure 4, where both the oxygen transport resistance and proton transport resistance are low, the reaction occurs at an intrinsic rate, and $F_e^{(C)}$ is close to 1. This graph more clearly demonstrates that, when one modulus is considerably higher than the other, the former determines $F_e^{(C)}$. In addition, when one of the dimensionless moduli is greater than 10, $F_e^{(C)}$ is less than approximately 0.1. Unfortunately, the effects of the two dimensionless moduli on $F_e^{(C)}$ are not even. $M_{O\,m}^{(C)}$ has a slightly greater impact than $M_{p\,m}^{(C)}$, as shown by the dense contours in the $M_{O\,m}^{(C)}$ direction and sparse contours in the $M_{p\,m}^{(C)}$ direction.

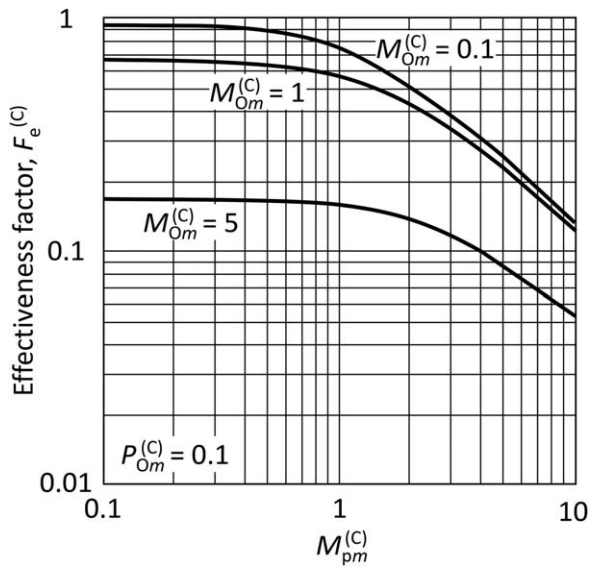

Figure 6. Effectiveness factor as a function of $M_{O\,m}^{(C)}$ and $M_{p\,m}^{(C)}$ ($P_{O\,m}^{(C)} = 0.1$).

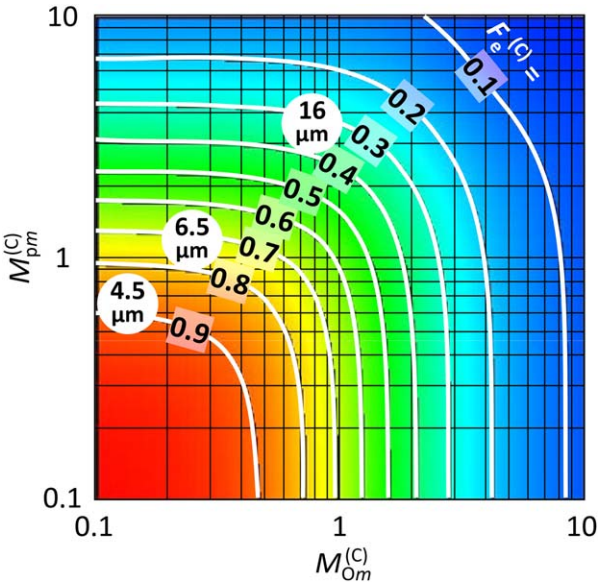

Figure 7. Effectiveness factor as a function of $M_{O\,m}^{(C)}$ and $M_{p\,m}^{(C)}$ ($P_{O\,m}^{(C)} = 0$).

[Color figure can be viewed at wileyonlinelibrary.com]

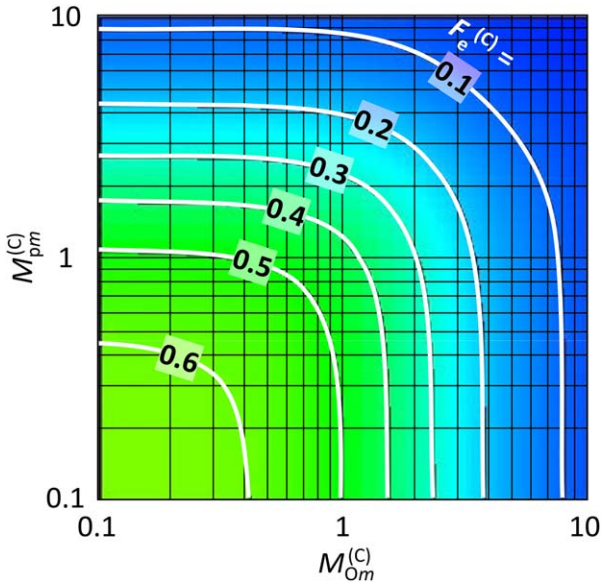

Figure 8. Effectiveness factor as a function of $M_{O\,m}^{(C)}$ and $M_{p\,m}^{(C)}$ ($P_{O\,m}^{(C)} = 1$).

[Color figure can be viewed at wileyonlinelibrary.com]

Compared with the effects of $M_{O\,m}^{(C)}$ and $M_{p\,m}^{(C)}$, the other two dimensionless parameters, $P_{O\,m}^{(C)}$ and y_{Oc}, have only moderate effects on $F_e^{(C)}$ under ordinary operating conditions. Although this study assumes an oxygen mole fraction, y_{Oc}, of 0.62 at the CL–GDL boundary (corresponding to an inlet gas consisting of undiluted oxygen humidified at 75°C), the value of y_{Oc} depends on the position in the cell, the geometry of the cell, and the operating conditions, such as the supply gas (oxygen or air), RH, and flow rate. In the numerical simulation of a whole cell, the y_{Oc} distribution is calculated using a model describing mass transport primarily in the GDL and flow channel.[10] As y_{Oc} is raised, the effects of oxygen convection appear greater. In the case of an air supply, a more typical y_{Oc} value is 0.1–0.21, and $F_e^{(C)}$ under such conditions will be greater than the results obtained in this study.

The values of $M_{O\,m}^{(C)}$ and $M_{p\,m}^{(C)}$ cannot be chosen independently in many actual cases. As an example, both of these terms will vary with the amount of ionomer in the cathode. Increases in the ionomer loading increase the effective proton conductivity and lower $M_{p\,m}^{(C)}$, but also reduce the effective O_2 diffusivity, thus raising $M_{O\,m}^{(C)}$. The values of $M_{O\,m}^{(C)}$ and $M_{p\,m}^{(C)}$ obtained with varying ionomer amounts describe a locus in a figure similar to Figures 7 and 8. Based on the $F_e^{(C)}$ contours, the optimal conditions are represented by a point on the locus where $F_e^{(C)}$ is highest.

Comparing Figures 6 and 7, calculated, respectively, at $P_{O\,m}^{(C)} = 0.1$ and 0, the $F_e^{(C)}$ values are seen to be similar to one another. However, if the Peclet number, $P_{O\,m}^{(C)}$, is greater than 0.1, the effects of convection cannot be neglected. The water flux through the PEM, $N_A^{(M)}$, varies remarkably depending on the humidification conditions and the current density, and the difference in the RH on either side of PEM governs the diffusion of moisture in the PEM. The proton current carries moisture by electroosmosis, which is why the value of $P_{O\,m}^{(C)}$ in actual cells ranges from approximately −3 to 6. The $F_e^{(C)}$ estimated at $P_{O\,m}^{(C)} = 1$ is shown in Figure 8, where it can be seen that, even at $(M_{p\,m}^{(C)}, M_{O\,m}^{(C)}) = (0.1, 0.1)$, $F_e^{(C)}$ is lower than 0.7 and approximately 0.7 times that at $P_{O\,m}^{(C)} = 0$. A positive Peclet number reduces the oxygen partial pressure in the CL, yielding a lower $F_e^{(C)}$. Conversely, a negative Peclet number represents an oxygen profile that is shifted toward the PEM side, resulting in an improved $F_e^{(C)}$. The importance of water management in such cells is well known, and is usually explained in terms of drying out of the PEM and flooding of the GDL. Water permeation through the PEM determines the Peclet number. Appropriate water management is also required with regard to optimizing the catalyst effectiveness factor.

As a final step, the operational conditions of the current PEFCs were estimated, assuming the reaction rate equation to be that given in Eq. 2, along with a cathode CL thickness of $\delta^{(C)} = 3$–16 μm and a platinum loading of 300 kg/m^3. The effective oxygen diffusivity is highly dependent on the CL structure and, assuming a porosity value of 0.5–0.6 and a tortuosity factor of 12–25, the effective oxygen diffusivity, D_{eO}, is on the order of 10^{-7} m^2/s.[11] The effective proton conductivity is estimated to be 1 S/m since the volume fraction of the ionomer in the CL is approximately 0.2 and the proton conductivity of the PEM is in the vicinity of 5 S/m.[12] In Figure 7, the circles show the estimated conditions for three different CL thicknesses: 4.5, 6.5, and 16 μm. The $F_e^{(C)}$ is approximately 0.3 for a typical CL thickness of 16 μm. If the thickness is reduced to 4.5 μm, $F_e^{(C)}$ is expected to be improved to approximately 0.9. These data indicate that $F_e^{(C)}$ can be improved by a factor of three through optimizing the CL, but that no further improvement is possible. Reducing the CL thickness while holding the other parameters constant lowers the overall reaction rate since the platinum loading is lowered, and so it is also necessary to improve one or more of the other parameters. These parameters are contained in the equations defining the dimensionless moduli, Eqs. 20 and 24. Furthermore, the extent of improvement that is required can only be determined by calculating these moduli. If the operating conditions change over time while driving a fuel cell vehicle or operating a residential fuel cell, the changes in $M_{O\,m}^{(C)}$ and $M_{p\,m}^{(C)}$ will form a locus, as in Figures 7 and 8. The bottleneck can be identified from these loci, which will assist in determining the cell factors that must be improved.

Conclusions

The ORR rate in the cathode CL of a PEFC was analyzed and a chemical reaction engineering model of the CL was developed. Since the rate of an electrochemical reaction is a function of the interfacial potential difference, reactant concentrations, and temperature, the actual rate of the reaction is determined by competition between the reaction, oxygen transport, and proton transport. The interfacial potential difference (that is, the cathode electromotive force) and temperature both determine the first-order reaction rate constant. As well, proton transport resistance affects the reaction rate not by reducing the proton concentration but rather by reducing the proton potential. Oxygen and protons enter the cathode from two opposite sides. The complex nature of such cells results in many degrees of freedom but, by employing dimensionless variables, the system was simplified to only five degrees of freedom. As well, it was demonstrated that just four dimensionless parameters govern the dimensionless reaction rate profile and the effectiveness factor. A dimensionless model analysis determined that the behavior of the cathode was well characterized by two of the dimensionless moduli proposed in this study, $M_{O\,m}^{(C)}$ and $M_{p\,m}^{(C)}$, in addition to the Peclet number,

$P_{\mathrm{O}\,m}^{(\mathrm{C})}$, and a boundary condition, y_{Oc}. These dimensionless moduli, $M_{\mathrm{O}\,m}^{(\mathrm{C})}$ and $M_{\mathrm{p}\,m}^{(\mathrm{C})}$, represent the ratios of reaction to oxygen transport and reaction to proton transport. The effects of $P_{\mathrm{O}\,m}^{(\mathrm{C})}$ were also assessed on the basis of the data produced in this work. In general, this study showed that a chemical reaction engineering approach is useful even when evaluating electrochemical reactions.

Acknowledgments

This work was supported by the Fuel Cell Cutting-edge Scientific Research Project (FY 2010–FY 2014) and the Highly-coupled Analysis of Phenomena in MEA and its Constituents and Evaluation of Cell Performance Project (FY 2015–FY 2017) conducted by the New Energy and Industrial Technology Development Organization (NEDO), Japan.

Literature Cited

1. Kawase M, Inagaki T, Miura K. Nonisothermal through-plane transport model of PEMFC with local VLE assumption. *ECS Trans*. 2008;16:563–573.
2. Weber A, Borup RL, Darling RM, Das PK, Dursch TJ, Gu W, Harvey D, Kusoglu A, Litster S, Mench MM, Mukundan R, Owejan JP, Pharoah JG, Secanell M, Zenyuk IV. A critical review of modeling transport phenomena in polymer-electrolyte fuel cells. *J Electrochem Soc*. 2014;161:F1254–F1299.
3. Poltarzewski Z, Staiti P, Alderucci V, Wieczorek W, Giordano N. Nafion distribution in gas diffusion electrodes for solid-polymer-electrolyte-fuel-cell applications. *J Electrochem Soc*. 1992;139:761–765.
4. Chin ST, Kawashima S, Kageyama M, Kawase M, Miura K. Analysis of the oxygen reduction reaction of a PEFC. *In Abstracts for 6th APCRE Symposium* (*Beijing*). Beijing, China: Chinese Academy of Sciences, 2011:A-5.
5. Nagayoshi M, Nobuta Y, Kageyama M, Inoue G, Kawase M. Rate of oxygen reduction reaction in the cathode catalyst layer of PEFC. *In World Congress on Chemical Engineering 9,* (*Seoul*). Seoul, Korea: The Korean Institute of Chemical Engineers, 2013:MoP-T1-170.
6. Kawase M, Nagayoshi M, Inoue G, Kageyama M. Dependency of oxygen reduction reaction rate on relative humidity in polymer electrolyte fuel cell. *In Proceedings of 23rd ISCRE & 7th APCRE Symposium* (*Bangkok*). Bangkok, Thailand: The Thai Institute of Chemical Engineering and Applied Chemistry, 2014:OE-03.
7. Sepa DB, Vojnovic MV, Vracar LM, Damjanovic A. Electro-oxidation mechanisms of methanol and formic acid on Pt-Ru alloy surfaces. *Electrochim Acta*. 1986;31:91–96.
8. Limjeerajarus N, Yanagimoto T, Yamamoto T, Ohashi H, Ito T, Yamaguchi T. Analysis of oxygen reduction reaction activity of Pt/C catalysts for actual PEFC MEAs. *J Chem Eng Japan*. 2009;42:39–46.
9. Zhukovsky K. Modeling of the current limitations of PEFC. *AIChE J*. 2006;52:2356–2366.
10. Benziger J, Kimball E, Mejia-Ariza R, Kevrekidis I. Oxygen mass transport limitations at the cathode of polymer electrolyte membrane fuel cells. *AIChE J*. 2011;57:2505–2517.
11. Inoue G, Kawase K, Yokoyama K, Oyama J, Terao T, Kubo N. Theoretical analysis of relationship between porous electrode structure and mass transfer performance for PEFCs by direct measurement and simulation. *In Abstracts of 228th ECS Meeting* (*Phoenix*). Pennington, NJ: The Electrochemical Society, 2015:#1285.
12. Springer TE, Zawodzinski TA, Gottesfeld S. Polymer electrolyte fuel cell model. *J Electrochem Soc*. 1991;138:2334–2342.

Manuscript received Apr. 4, 2016, and revision received Sep. 20, 2016.